

Supplementary Information for:

A Flexible Iron(II) Complex in which Zero-Field Splitting is Resistant to Structural Variation

Joseph M. Zadrozny,¹ Samuel M. Greer,^{2,3} Stephen Hill,^{3,4} and Danna E.

Freedman^{1*}

¹ *Department of Chemistry, Northwestern University, Evanston, Illinois 60208*

² *Department of Chemistry and Biochemistry, Florida State University, Tallahassee, FL, 32310, USA.*

³ *National High Magnetic Field Laboratory, Tallahassee, FL, 32310, USA.*

⁴ *Department of Physics, Florida State University, Tallahassee, FL, 32310, USA.*

Table of Contents

Full Experimental Details	S3
Equations for spin-allowed contributions to D and E in a d^6 complex.	S7
Table S1. Full Crystal Table for 1	S8
Table S2. Full Crystal Table for 2 .	S9
Table S3. Full Crystal Table for 3 .	S10
Figure S1. Experimental thermal ellipsoids for the structures of $[\text{Fe}(\text{C}_3\text{S}_5)_2]^{2-}$ in 1-3 .	S11
Figure S2. Packing diagrams for 1 , 2 , and 3 .	S12
Figure S3. Variable-temperature, variable-field dc susceptibility data for 1-3 and fits.	S13
Figure S4. Select high-frequency EPR spectra and simulations for 1-3 .	S14
Figure S5. Frequency dependence of resonant fields for 2 and 3 .	S15
Figure S6. Zeeman energy diagrams based on best fits for 1 .	S16
Figure S7. Low-temperature magnetization data for 1-3 .	S17
References	S18

Full Experimental Details.

General Considerations. Manipulations of all compounds were performed under a dinitrogen atmosphere in a Vacuum Atmospheres Nexus II glovebox. Glassware was either oven-dried at 150 °C for at least 4 hours or flame-dried prior to use. Acetonitrile (MeCN), diethylether (Et₂O), tetrahydrofuran (THF), and methanol (MeOH) were dried using a commercial solvent purification system from Pure Process Technology and stored over 3 or 4 Å sieves prior to use. Immediately prior to use, Et₂O and THF were subjected to tests with a standard purple solution of sodium benzophenone ketyl in THF to confirm low O₂ and H₂O content. 4,5-dibenzoyl-1,3-dithiole-1-thione (PhCO)₂(C₃S₅) was prepared following the literature procedure.¹ 18-crown-6 was recrystallized from MeCN and dried at 50 °C overnight. All other reagents were used as received.

[(18c6)K]₂[Fe(C₃S₅)₂] (1). A mixture of (PhCO)₂(C₃S₅) (230 mg, 0.566 mmol) and KOMe (79 mg, 1.5 mmol) were stirred in 10 mL of methanol until a clear dark red solution was obtained. A solution of FeCl₂ (35 mg, 0.28 mmol) in 2 mL of methanol was added, yielding a dark red-orange solution, which was allowed to stir ca. one hour. A solution of 18-crown-6 (147 mg, 0.597 mmol) in 2 mL of methanol was added, and the solution was allowed to stir overnight. Subsequently, 20 mL of THF were added to the resulting red residue. The mixture was stirred briefly, then pumped down to dryness *in vacuo* followed by further drying at 65 °C for 2 h. This procedure was repeated twice. Finally, the mixture was dissolved in 40 mL of THF and filtered to afford a dark red solution. Diethyl ether vapor was allowed to diffuse into this mother liquor overnight, yielding red, needle-like crystals of **1** (142 mg, 48 %). IR(cm⁻¹):2896(m), 1469(w), 1421(m), 1348(m), 1281(w), 1244(w), 1106(vs), 1048(s), 1028(s), 990(w), 961(s), 893(w), 837(m), 521(m), 458(s). ESI/MS (*m/z*): {Fe(C₃S₅)₂}⁻, 447.657 (base). Anal. Calcd. for C₃₀H₄₈FeK₂O₁₂S₁₀•3(C₄H₈O): 39.67 %C; 5.71 %H. Found: 39.76 %C; 5.63 %H.

(Ph₄P)₂[Fe(C₃S₅)₂] (2). Solid (PhCO)₂(C₃S₅) (192 mg, 0.472 mmol) and NaOMe (50 mg, 0.93 mmol) were stirred in 10 mL of MeOH until a clear dark red solution was obtained. A solution of FeCl₂ (29 mg, 0.23 mmol) in 2 mL of MeOH was added and the resulting dark red orange solution was allowed to stir 3 h. A solution of (Ph₄P)Br (194 mg, 0.463 mmol) in 2 mL of MeOH was added dropwise over the course of a minute with vigorous stirring, producing a red microcrystalline solid by the end of the addition. The mixture was kept at -35 °C overnight, then

filtered to collect the red crystalline solid and briefly dried. The solid was then recrystallized from 40 mL of hot MeCN (193 mg, 75 %). IR(cm^{-1}): 3047 (w), 3012 (w), 2986 (w), 2959 (w), 2922 (w), 1583 (s), 1482 (s), 1343 (vs), 1407 (vs), 1364 (w), 1337 (m), 1314 (m), 1186 (m), 1105 (vs), 1051 (s), 1025 (vs), 994 (vs), 977 (w), 891 (s), 849 (w), 752 (s), 718 (vs), 684 (vs), 615 (w), and 520 (vs). ESI/MS (m/z): $\{\text{Fe}(\text{C}_3\text{S}_5)_2\}^-$, 447.645 (base); $\{(\text{Ph}_4\text{P})[\text{Fe}(\text{C}_3\text{S}_5)_2]\}^-$ 786.827. Anal. Calcd. for $\text{C}_{54}\text{H}_{40}\text{P}_2\text{S}_{10}\text{Fe}\cdot\text{CH}_3\text{CN}$: 57.57 %C; 3.71 %H; 1.20 %N. Found: 57.30 %C; 3.51 %H; 1.18 %N.

(Bu₄N)₂[Fe(C₃S₅)₂] (3). Solid $(\text{PhCO})_2(\text{C}_3\text{S}_5)$ (203 mg, 0.499 mmol) and NaOMe (54 mg, 1.0 mmol) were stirred in 10 mL of MeOH until a clear dark red solution was obtained. To this solution a solution of FeCl_2 (31 mg, 0.24 mmol) in 2 mL of MeOH was added and the resulting dark red orange solution was allowed to stir 45 m. A solution of $(\text{Bu}_4\text{N})\text{Br}$ (160 mg, 0.496 mmol) in 2 mL of MeOH was added dropwise and the mixture was allowed to stir 15 m prior to being stored at $-35\text{ }^\circ\text{C}$ for 2d. The resulting red microcrystalline solid was redissolved in 10 mL of MeCN and layered under 30 mL of Et_2O to afford dark red crystals of **3** (122 mg, 54 %). IR(cm^{-1}): 2959(m), 2871(w), 1460(m), 1413(s), 1381(w), 1176(w), 1153(w), 1109(w), 1054(s), 1029(vs), 991(m), 897(w), 881(m), 802(w), 741(m), 526(m), 460(vs). ESI/MS (m/z): $\{\text{Fe}(\text{C}_3\text{S}_5)_2\}^-$, 447.647 (base). Anal. Calcd. for $\text{C}_{38}\text{H}_{72}\text{N}_2\text{FeS}_{10}$: 48.90 %C; 7.78 %H. Found: 48.63 %C; 7.48 %H.

X-ray Data Collection, Structure Solution and Refinement for 1-3. Data collection was performed on a single crystal coated in Paratone-N oil and mounted on a MicroMountsTM rod under a freezing stream of N_2 . During mounting, crystals of **1-3** did not show any signs of desolvation or other decomposition. Data were collected for **1-3** using a Bruker KAPPA diffractometer equipped with a Mo $\text{K}\alpha$ ($\lambda = 0.71073\text{ \AA}$) sealed-tube X-ray source, an APEX-II detector, and Oxford Cryosystems Cryostream cryostat. Raw data were integrated and corrected for Lorentz and polarization effects using Bruker Apex2 v. 2013.2.² Absorption corrections were applied using SADABS.³ The space group was determined by examination of systematic absences, E-statistics, and successive refinement of the structure. The crystal structure was solved with direct methods and further refined with SHELXL⁴ operated with the OLEX2 interface.⁵ The crystal did not show significant decay during data collection. Thermal parameters were refined anisotropically for all non-hydrogen atoms or ions in **1-3** except for light atoms

modeled as disordered. Disordered solvent molecules, where present, were modeled with the use of free variables. Hydrogen atoms were placed in ideal positions and refined using a riding model for all structures. Full crystal tables for **1-3** are given in Tables S1-S3. Crystallographic information files (cifs) for **1-3** can be obtained from the Cambridge Structural Database with refcodes CCDC 1064089-1064091.

Magnetic Measurements. All samples were prepared under an inert atmosphere. Magnetic measurements of **1** and **3** were performed on polycrystalline samples in either flame-sealed quartz tubes under vacuum or polycarbonate gelcaps. All samples were treated with molten eicosane to remove the possibility of crystallite torquing. Data were collected with a Quantum Design MPMS-XL SQUID magnetometer from 1.8 to 300 K and applied direct-current (dc) fields of 0 to 7 T. Dc susceptibility data were corrected for diamagnetic contributions from the sample holder and the core diamagnetism of the sample itself, estimated from Pascal's constants. Prior to full characterization, magnetization versus applied dc field curves from 0 to 4 T were collected for each sample to ensure the absence of curvature associated with ferromagnetic impurities. Data agreement was checked over multiple different measurements. Fits and simulations of magnetic susceptibility and magnetization data were performed with the Magprop package within DAVE⁶ and ANISOFIT 2.0,⁷ respectively.

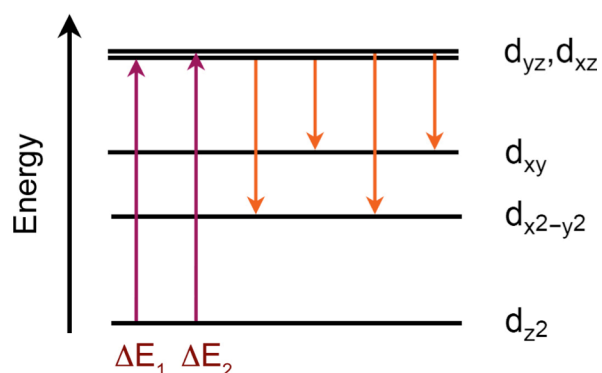
Zero-field ⁵⁷Fe Mössbauer Spectroscopic Measurements. All measurements were performed under zero applied magnetic field and at 80 K on ca. 40 (**1**), 90 (**2**), and 100 (**3**) mg of ground, microcrystalline samples. Samples were loaded into a circular plastic cap of 1 cm² area under an inert atmosphere and transferred quickly to the cryostat to avoid sample decomposition owing to air sensitivity. Spectra were collected with a constant acceleration spectrometer and a ⁵⁷Co/Rh source. Prior to measurements, the spectrometer was calibrated at 295 K with α -Fe foil. Spectra were analyzed using the WMOSS Mössbauer Spectral Analysis Software (www.wmoss.org).

Electron Paramagnetic Resonance. High-field, high-frequency EPR spectra were collected at temperatures from 5 to 15 K with a home-built transmission spectrometer at the Electron Magnetic Resonance facility of the National High Magnetic Field Laboratory. The specifications of this instrument are described elsewhere.⁸ Samples were thoroughly ground microcrystalline powders, restrained in paratone n-oil and sealed in plastic holders following reported suggested guidelines.⁹ As shown in the EPR spectra (Figs. 2, S3) and resonant field v. frequency (Figs. 3,

S4) plots, the z -components for the transitions are either weak or otherwise obscured by a background feature.

Other Physical Measurements. Combustion analyses were performed by Midwest Microlab (Indianapolis, IN). Infrared spectra were recorded on a Bruker Alpha FTIR spectrometer equipped with an attenuated total reflectance accessory. Electrospray ionization mass spectrometry measurements were performed on acetonitrile solutions of **1-3** with a Bruker Amazon X ESI-Ion Trap Mass Spectrometer at the IMSERC facility of Northwestern. Compounds **1-3** were prepared for powder X-ray diffraction experiments under an inert atmosphere and placed in Anton Paar domed sample holders for measurement. Powder X-ray diffraction experiments to connect bulk purity with the single-crystal structures were performed with Cu K α ($\lambda = 1.541\ 78\ \text{\AA}$) radiation on a PANalytical Empyrean diffractometer with a PIXcel 1D detector. Powder patterns were baseline-corrected for the amorphous signal of the domed sample holder and normalized with HighScore Plus v. 3.0.5 (PANalytical, 2012). Simulated powder patterns were calculated with Mercury and the single-crystal structures.¹⁰

Additional details regarding the zero-field splitting of $[\text{Fe}(\text{C}_3\text{S}_5)_2]^{2-}$. The figure below is an expanded version of panel c in Fig. 5. This expanded version indicates the d-d transitions that



are spin allowed (red) and spin-flip (orange) transitions, which have nonzero contributions to D and E . Formulae for the contributions to D and E from a given excited state here were determined following the methods summarized by Dai et al. and assuming that the d-orbitals are pure and un-mixed.¹¹ Spin-allowed contributions to D and E are described in terms of ΔE_1 and ΔE_2 :

$$D_{spin\ allowed} = \frac{3\zeta^2}{32} \left(\frac{1}{\Delta E_1} + \frac{1}{\Delta E_2} \right), E_{spin\ allowed} = \frac{3\zeta^2}{32} \left(\frac{1}{\Delta E_1} - \frac{1}{\Delta E_2} \right)$$

Here ζ is the free ion spin-orbit coupling constant, and $\Delta E_{1,2}$ represents the energy gap between the ground and excited state of the labeled d-d transition. From this equation, it is clear why a distortion that shifts the d_{xz} and d_{yz} orbitals away from degeneracy induces a nonzero value of E . However, even for the highly symmetric species **1**, use of the D and E values obtained from EPR spectra reveal ΔE_1 and ΔE_2 to be 5604 cm^{-1} and 6977 cm^{-1} , which yields a 1372 cm^{-1} gap between the d_{xz} and d_{yz} orbitals. The unexpectedly large gap obtained from this method suggests a spin-allowed model is too simple to determining D and E . In addition, the assumption of d-orbital purity conflicts with other models that allow for mixing of the ground d_{z^2} orbital with the $d_{x^2-y^2}$ orbital,¹² which may further give rise to the discrepancy. In time, computational studies will hopefully resolve these questions.

Table S1 | Crystallographic information for the structural refinement of **1**.

Empirical Formula	$C_{42}H_{72}FeK_2O_{15}S_{10}$
Formula weight	1271.65 g/mol
Temperature	100(2) K
Wavelength	0.71073 Å
Crystal System	Monoclinic
Space Group	<i>Pn</i>
Unit Cell Dimensions	$a = 9.6660(4)$ Å, $\alpha = 90^\circ$ $b = 17.7362(8)$ Å, $\beta = 104.302(2)^\circ$ $c = 17.9259(7)$ Å, $\gamma = 90^\circ$
Volume	2977.9(2) Å ³
Z	2
Density (calculated)	1.418 Mg/m ³
Absorption coefficient	0.801 mm ⁻¹
F_{000}	1336
Crystal color	Dark red
Crystal size	0.27 × 0.16 × 0.11 mm ³
θ range	1.15 to 26.42°
Index ranges	$-12 \leq h \leq 12$ $-22 \leq k \leq 22$ $-19 \leq l \leq 22$
Reflections collected	52038
Independent reflections	11046 [$R_{\text{int}} = 0.0314$]
Completeness to $\theta = 26.42^\circ$	99.9 %
Absorption correction	Multi-scan
Maximum and minimum transmission	0.910 and 0.857
Refinement method	Full-matrix least-squares on F^2
Data / restraints / parameters	11046 / 26 / 623
Goodness-of-fit on F^{2a}	1.158
Final R indices [$I > 2\sigma(I) = 11046$ data] ^b	$R_1 = 3.29$ %, $wR_2 = 8.52$ %
R indices (all data, 0.81 Å)	$R_1 = 4.25$ %, $wR_2 = 12.17$ %
Largest diff. peak and hole	0.513 and -0.675 e.Å ⁻³

^a GooF = $[\sum[w(F_o^2 - F_c^2)^2] / (n-p)]^{1/2}$ where n is the number of reflections and p is the total

number of parameters refined. ^b $R_1 = \sum||F_o| - |F_c|| / \sum|F_o|$; $wR_2 = [\sum[w(F_o^2 - F_c^2)^2] / \sum[w(F_o^2)^2]]^{1/2}$

Table S2 | Crystallographic information for the structural refinement of **2**.

Empirical Formula	$C_{56}H_{43}FeNP_2S_{10}$
Formula weight	1168.40 g/mol
Temperature	100(2) K
Wavelength	0.71073 Å
Crystal System	Triclinic
Space Group	$P\bar{1}$
Unit Cell Dimensions	$a = 9.5532(3)$ Å, $\alpha = 64.7735(7)^\circ$ $b = 16.9392(6)$ Å, $\beta = 78.6184(8)^\circ$ $c = 19.2199(7)$ Å, $\gamma = 78.0782(8)^\circ$
Volume	2731.85(16) Å ³
Z	2
Density (calculated)	1.420 Mg/m ³
Absorption coefficient	0.756 mm ⁻¹
F_{000}	1204
Crystal color	Dark red
Crystal size	0.29 × 0.19 × 0.19 mm ³
θ range	2.36 to 26.00°
Index ranges	$-11 \leq h \leq 11$ $-20 \leq k \leq 20$ $-23 \leq l \leq 23$
Reflections collected	10782
Independent reflections	9165 [$R_{\text{int}} = 0.0330$]
Completeness to $\theta = 26.00^\circ$	99.0 %
Absorption correction	Multi-scan
Maximum and minimum transmission	0.801 and 0.764
Refinement method	Full-matrix least-squares on F^2
Data / restraints / parameters	10673 / 7 / 646
Goodness-of-fit on F^{2a}	1.036
Final R indices [$I > 2\sigma(I) = 10673$ data] ^b	$R_1 = 2.52$ %, $wR_2 = 5.74$ %
R indices (all data, 0.80 Å)	$R_1 = 3.30$ %, $wR_2 = 6.11$ %
Largest diff. peak and hole	0.483 and -0.273 e.Å ⁻³

^a GooF = $[\sum[w(F_o^2 - F_c^2)^2] / (n-p)]^{1/2}$ where n is the number of reflections and p is the total

number of parameters refined. ^b $R_1 = \sum||F_o| - |F_c|| / \sum|F_o|$; $wR_2 = [\sum[w(F_o^2 - F_c^2)^2] / \sum[w(F_o^2)^2]]^{1/2}$

Table S3 | Crystallographic information for the structural refinement of **3**.

Empirical Formula	C ₃₈ H ₇₂ FeN ₂ S ₁₀
Formula weight	933.43 g/mol
Temperature	100(2) K
Wavelength	0.71073 Å
Crystal System	Triclinic
Space Group	<i>P</i> 2 ₁ / <i>c</i>
Unit Cell Dimensions	<i>a</i> = 8.5730(5) Å, α = 90° <i>b</i> = 32.0602(17) Å, β = 98.509(3)° <i>c</i> = 17.6411(9) Å, γ = 90°
Volume	4795.3(5) Å ³
<i>Z</i>	4
Density (calculated)	1.293 Mg/m ³
Absorption coefficient	0.778 mm ⁻¹
<i>F</i> ₀₀₀	2000
Crystal color	Red
Crystal size	0.30 × 0.23 × 0.17 mm ³
θ range	1.27 to 26.02°
Index ranges	-10 ≤ <i>h</i> ≤ 10 -38 ≤ <i>k</i> ≤ 39 -21 ≤ <i>l</i> ≤ 21
Reflections collected	87156
Independent reflections	9433 [<i>R</i> _{int} = 0.0885]
Completeness to θ = 26.02°	99.9 %
Absorption correction	Multi-scan
Maximum and minimum transmission	0.704 and 0.641
Refinement method	Full-matrix least-squares on <i>F</i> ²
Data / restraints / parameters	9433 / 0 / 468
Goodness-of-fit on <i>F</i> ^{2a}	1.094
Final <i>R</i> indices [<i>I</i> > 2σ(<i>I</i>) = 10626 data] ^b	<i>R</i> ₁ = 3.34 %, <i>wR</i> ₂ = 7.72 %
<i>R</i> indices (all data, 0.80 Å)	<i>R</i> ₁ = 4.51 %, <i>wR</i> ₂ = 8.9419 %
Largest diff. peak and hole	0.399 and -0.261 e.Å ⁻³

^a GooF = $[\sum[w(F_o^2 - F_c^2)^2] / (n-p)]^{1/2}$ where *n* is the number of reflections and *p* is the total

number of parameters refined. ^b*R*₁ = $\sum||F_o| - |F_c|| / \sum|F_o|$; *wR*₂ = $[\sum[w(F_o^2 - F_c^2)^2] / \sum[w(F_o^2)^2]]^{1/2}$

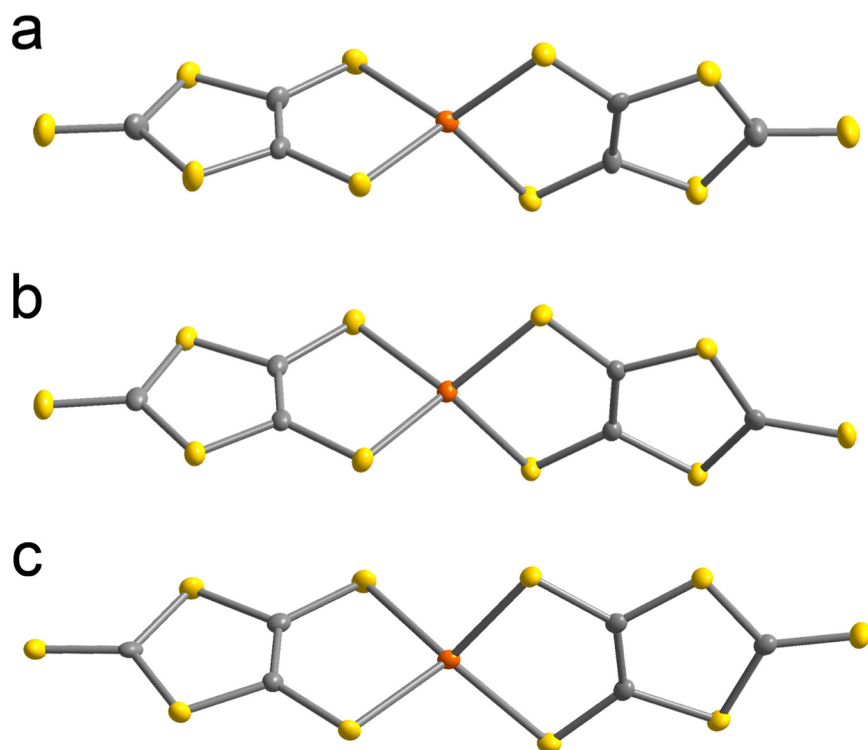


Figure S1 | Thermal ellipsoid plots of $[\text{Fe}(\text{C}_3\text{S}_5)_2]^{2-}$ in 1 (a), 2 (b), and 3 (c) drawn at the 50 % probability level. Orange, yellow, and gray ellipsoids correspond to Fe, S, and C atoms, respectively.

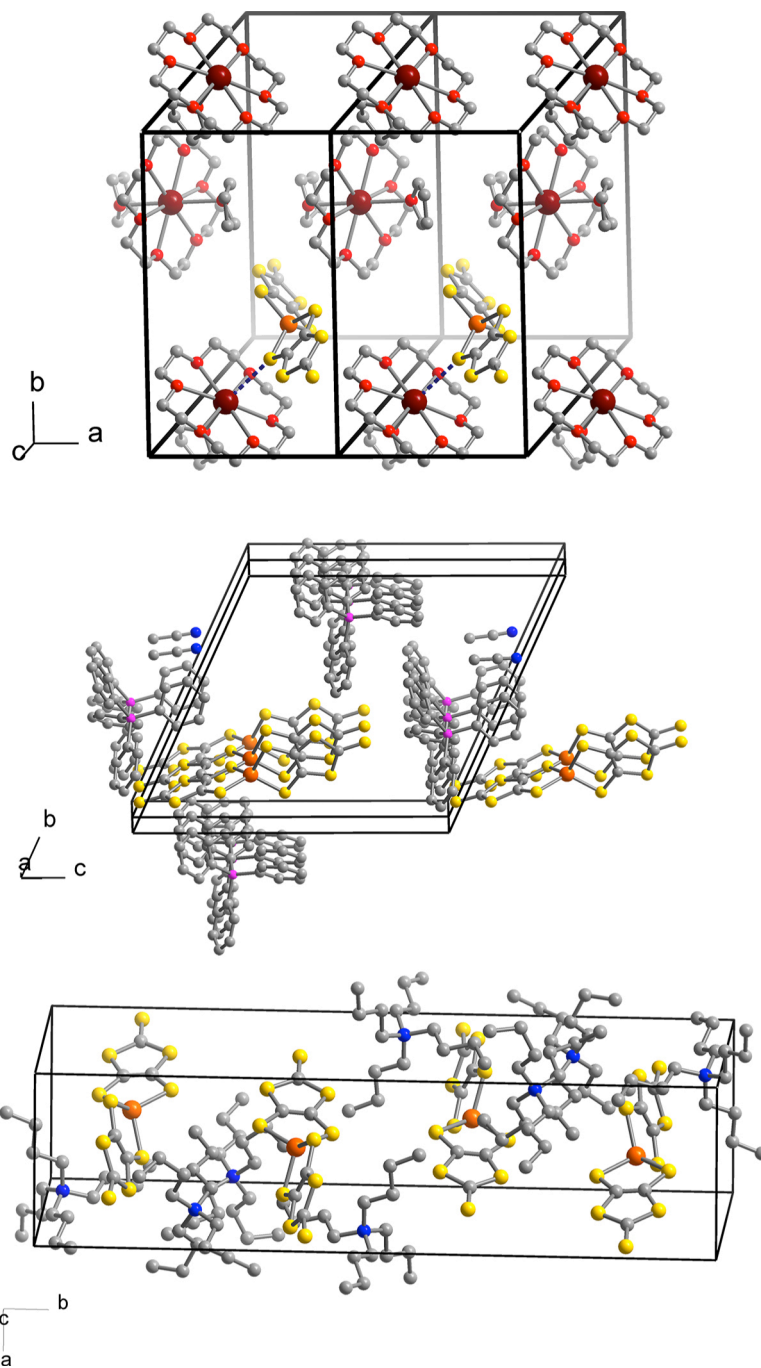


Figure S2 | Packing diagrams for 1 (top), 2 (middle), and 3 (bottom). Orange, dark red, yellow, pink, red, blue and gray ellipsoids correspond to Fe, K, S, P, O, N, and C atoms, respectively.

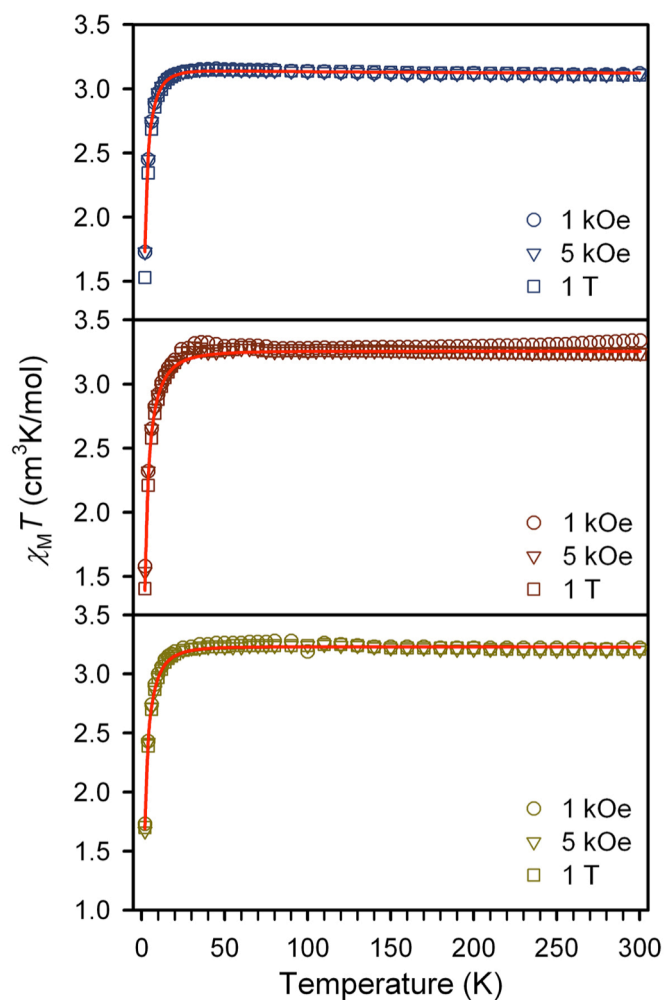


Figure S3 | Variable-temperature dc magnetic susceptibility data for 1 (top, blue), 2 (dark red, middle), and 3 (dark yellow, bottom) under three different applied dc fields. Data were collected on restrained polycrystalline powders sealed under vacuum in quartz tubes. Bright red lines indicate simulated data based on the average g_{iso} , D , and E values obtained from the best fits to the 1 kOe, 5 kOe, and 1 T data. These parameters are as follows: For **1**, $g_{\text{iso}} = 2.04(1)$, $D = +5.6(1) \text{ cm}^{-1}$, and $|E| = 0.5(3) \text{ cm}^{-1}$. For **2**, $g_{\text{iso}} = 2.08(2)$, $D = +6.5(3) \text{ cm}^{-1}$, and $|E| = 0.7(2) \text{ cm}^{-1}$. Finally, for **3**, $g_{\text{iso}} = 2.07(1)$, $D = +5.5(2) \text{ cm}^{-1}$, and $|E| = 0.7(1) \text{ cm}^{-1}$.

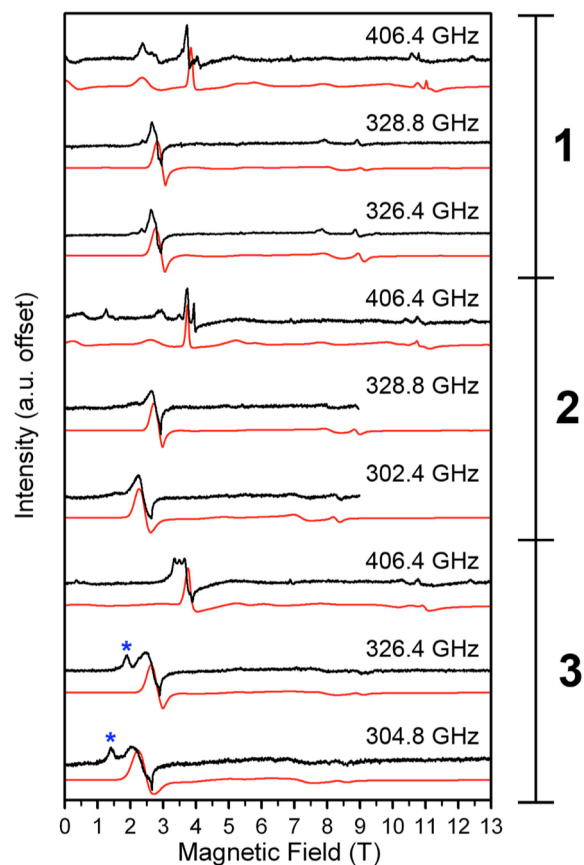


Figure S4 | Selected continuous-wave EPR spectra and simulations for 1-3. Spectra were collected on ground powders. Simulations were afforded using the parameters given in Table 2 of the main report. Blue asterisks in the spectra for **3** indicate peaks attributed to impurities. Simulations were obtained with $[D, E]$ strains (in cm^{-1}) of: $[0.22, 0.24]$, $[0.26, 0.22]$, $[0.35, 0.32]$ for **1**, **2**, and **3**, respectively.

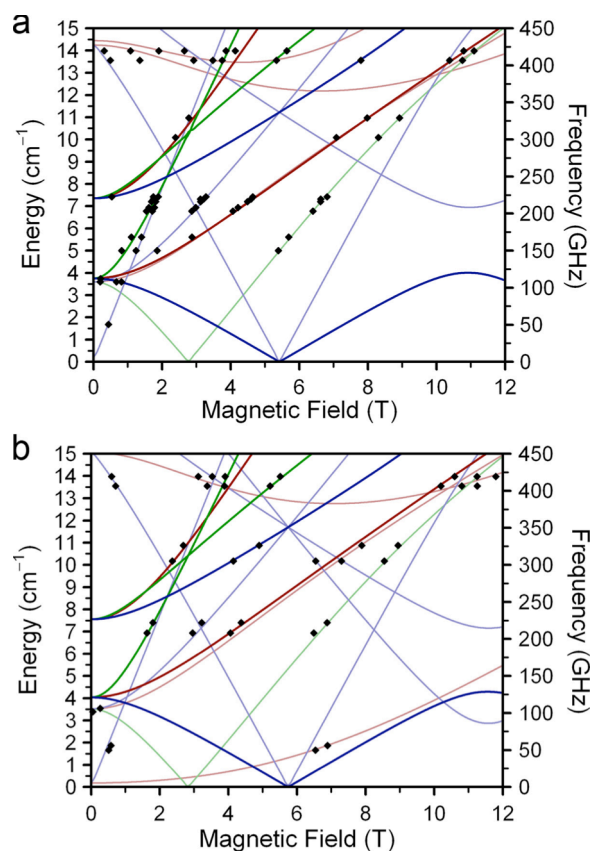


Figure S5 | Resonant field dependence vs. microwave frequency for 2 (a) and 3 (b). Plots were constructed from data (◆) obtained at 5 K. Solid lines represent fits to the data, with parameters as given in Table 2 of the main text. Red, green, and blue lines represent x -, y -, and z -transitions, respectively. Bold lines represent ground-state $M_S = 0 \rightarrow M_S = \pm 1$ transitions. Faded lines depict excited state transitions; those stemming from ca. 3.6 cm^{-1} correspond to excitations within the $M_S = \pm 1$ doublet. Excited state transitions are shown only if they potentially correspond to observed signals. Note that the transition labels here are based on the identities of the M_S levels in the high-field regime; at the field/frequency range of our current investigation, the M_S levels are significantly mixed.

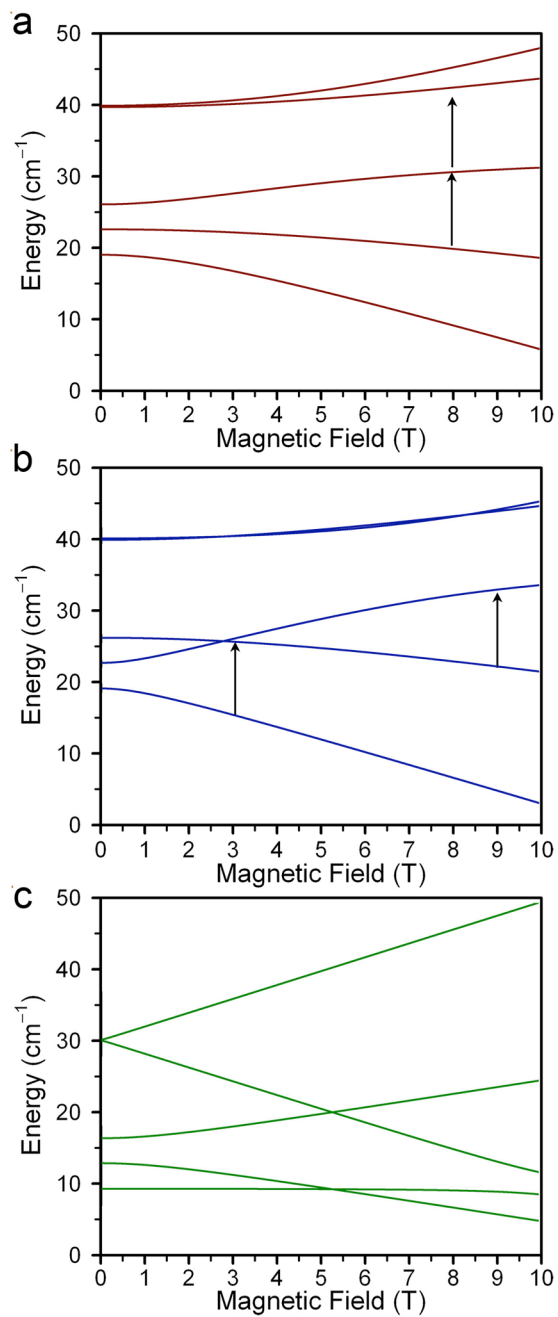


Figure S6 | Zeeman splitting diagrams for 1 calculated with the g , D , and E determined via fitting. The three graphs correspond to a magnetic field alignment along x (a), y (b), and z (c) axes, respectively. Black arrows in panels b and c indicate the parentage of the transitions observed in the 326.4 GHz EPR spectra depicted for 1 in Figs. 2 and 4 of the main report.

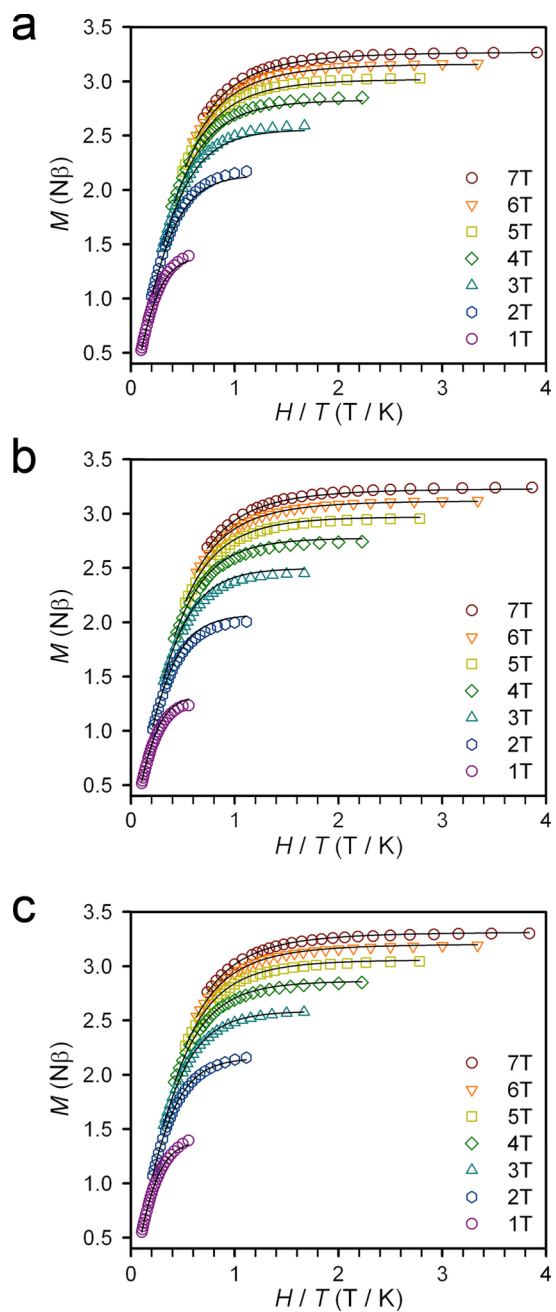


Figure S7 | Variable-temperature, variable-field magnetization data for 1(a), 2(b), and 3(c). Black lines are simulations of the magnetic data using the same g , D , and E values as the analysis of the EPR spectra. Simulations employed isotropic g_{iso} values obtained by averaging the g_x , g_y , and g_z components.

References:

1. T. Hansen, J. Becher, T. Jorgensen and K. Varma, *Org. Synth.* 1996, **73**, 270.
2. *APEX2*, v. 2009 ; Bruker Analytical X-Ray Systems, Inc: Madison, WI, 2009.
3. G. M. Sheldrick, *SADABS*, Version 2.03; Bruker Analytical X-Ray Systems, Inc.: Madison, WI, 2000.
4. G. M. Sheldrick, , *SHELXTL*, Version 6.12; Bruker Analytical X-ray Systems, Inc.: Madison, WI, 2000
5. O. V. Dolomanov, L. J. Bourhis, R. J. Gildea, J. A. K. Howard, and H. Puschmann, *J. Appl. Cryst.* 2009, **42**, 339-341.
6. *DAVE: A comprehensive software suite for the reduction, visualization, and analysis of low energy neutron spectroscopic data*, R. T. Azuah, L. R. Kneller, Y. Qiu, P. L. W. Tregenna-Piggot, C. M. Brown, J. R. D. Copley, and R. M. Dimeo, *J. Res. Natl. Inst. Stan. Technol.* 2009, **114**, 341-358.
7. M. P. Shores, J. J. Sokol, and J. R. Long, *J. Am. Chem. Soc.* 2002, **124**, 2279-2292.
8. A. K. Hassan, L. A. Pardi, J. Krzystek, A. Sienkiewicz, P. Goy, M. Rohrer and L.-C. Brunel *J. Magn. Reson.* 2000, **142**, 300-312.
9. J. Krzystek, A. Ozarowski, J. van Tol, J. Liu and S. Hill *EPR newsletter* 2012, **22**, 12.
10. C. F. Macrae, I. J. Bruno, J. A. Chisholm, P. R. Edgington, P. McCabe, E. Pidcock, L. Rodriguez-Monge, R. Taylor, J. van de Streek and P. A. Wood, *J. Appl. Cryst.* 2008, **41**, 466-470.
11. D. Dai, H. Xiang and M.-H. Whangbo, *J. Comput. Chem.* 2008, **29**, 2187-2209.
12. A. Abragam and B. Bleaney, *Electron Paramagnetic Resonance of Transition Ions*, Dover Publications, Inc., New York, 1986.